The tetragonal-to-orthorhombic phase transition in $RbAlF_4$: an X-ray scattering study

1990 J. Phys.: Condens. Matter 2 10549

(http://iopscience.iop.org/0953-8984/2/51/025)

J. Phys.: Condens. Matter 2 (1990) 10549–10558. Printed in the UK

The tetragonal-to-orthorhombic phase transition in $RbAlF_4$: an x-ray scattering study

F Brunet†, D F McMorrow‡, A Gibaud† and C Patterson‡

† Laboratoire de Physique de L'Etat Condensé, Université du Maine, 72017 Le Mans Cédex, France

‡ Department of Physics, University of Edinburgh, Edinburgh EH9 3JZ, UK

Received 17 August 1990

Abstract. The tetragonal-to-orthorhombic phase transition in $RbAlF_4$ at ≈ 290 K has been investigated using x-ray scattering techniques. For temperatures above ≈ 290 K, the wavevector dependence of the critical scattering at the X point was measured and was well described by an anisotropic Lorentzian, with no evidence for a second Lorentzian-squared component as has recently been reported close to the anti-ferrodistortive transition in several perovskites. The critical exponents describing the temperature dependence of the primary and secondary order parameters, inverse correlation length and static susceptibility were determined and found to be consistent with those expected for the isotropic $n = 2$, $d = 3$ model.

1. Introduction

Renewed interest in the study of x-ray critical scattering associated with displacive phase transitions has been stimulated largely by recent advances in x-ray instrumentation, most notably the development of the triple-crystal diffractometer. In Edinburgh these studies have focused mainly on the perovskites $SrTiO_3$ [1, 2], $RbCaF_3$ [3–5] and $KMnF_3$ [6]. The initial motivation for this work was to examine the x-ray critical scattering from the R-point soft mode in these materials, so as to complement the considerable body of neutron scattering data. However, it was soon discovered [1–6] that the critical fluctuations occur on two length scales, and not on one length scale as expected from the soft-mode theory of structural phase transitions [7]. It has been shown that the broader of the two components arises from the R-point soft mode, and that the existence of the sharper second is probably related to the presence of defects in the samples. Currently, there is no quantitative theory to account for all of the properties of the second length, and in particular its relationship to the central peak observed in neutron scattering is far from clear. We considered that it would be interesting to extend these studies to another class of materials, both to examine their intrinsic critical behaviour and to search for any evidence of a second length scale.

The tetrafluoroaluminates ABF_4, where A $\equiv$ (NH_4, Rb, K, Tl) and B $\equiv$ (Al, Fe), are layered compounds which display a rich variety of structural phase transitions. One of the archetypical structures, the so-called ideal phase (denoted as phase I), is found in the high-temperature phases of $TlAlF_4$ and $RbAlF_4$ and is characterised by layers of AlF_6^- octahedra, separated in the direction normal to the layers by the A cations (see figure 1). The structural phase transitions displayed by these compounds

0953-8984/90/5110549+10$03.50

are produced mainly by the correlated rotation of the rigid AlF_6^- octahedra [8], in a similar way to the phase transitions observed in perovskites; for example, the 105 K transition in $SrTiO_3$ is related to rotation of oxygen octahedra. However, the variety of structural phase transitions is greater in the ABF_4 family than in the perovskites, since depending upon the A cation it is possible to observe displacive [9, 10], martensitic [11, 12] or order–disorder [13] transitions.

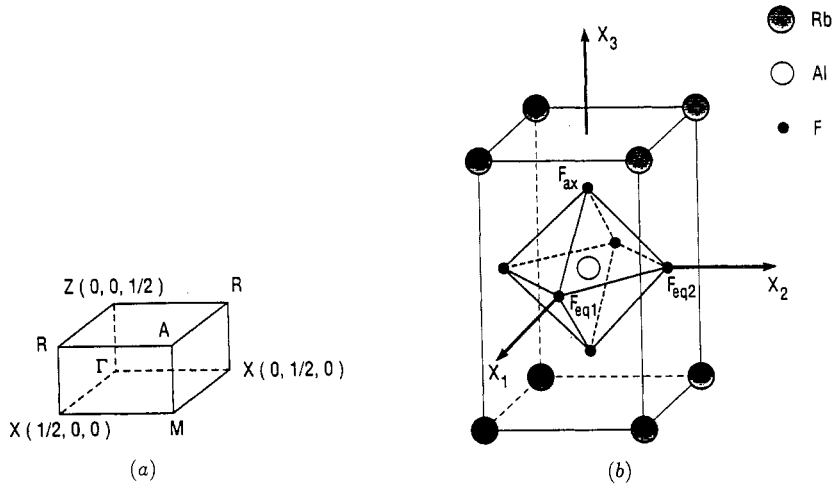

Figure 1. (*a*) The phase I Brillouin zone of $RbAlF_4$ and (*b*) its unit cell.

$RbAlF_4$ undergoes two structural phase transitions [9, 10]. The higher-temperature transition ($T_{C1} \approx 553$ K) is first order and non-ferroic, altering on cooling through T_{C1} the tetragonal space group from D_{4h}^1 (phase I) to D_{4h}^5 (phase II). The signature of the transition is the appearance below T_{C1} of superlattice reflections at the M point in the Brillouin zone of phase I, caused by the correlated rotation of AlF_6^- octahedra around the [001] axis (z axis). At $T_{C2} \approx 290$ K, a second order transition transforms phase II into an orthorhombic lattice (phase III, space group D_{2h}^{13}). This improper ferroelastic transition is caused by rotations of AlF_6^- octahedra around either the [100] or the [010] directions of phase I and a translation of the Rb^+ ions along the z axis. As the AlF_6^- octahedra can rotate around either the [100] or the [010] directions, this transition is characterised by a softening of a doubly degenerate mode at the X point of phase I (see figure 1).

In this paper we present the results of an x-ray scattering study of the tetragonal-to-orthorhombic transition in $RbAlF_4$ at T_{C2}. In addition to studying the critical x-ray scattering, particular attention was paid to measurement of the temperature dependence of the ferroelasticity below T_{C2}. Indeed, it is known that in this system that the spontaneous strain below T_{C2} is extremely small, and prior to this study a complete description of it was not available.

2. Experimental procedure

Our measurements were performed using a triple-crystal x-ray diffractometer situated on a GEC Avionics GX21 rotating anode generator. The high wavevector resolution required for the measurements of the spontaneous strain was achieved using identical

germanium (111) crystals to monochromate Cu $K_{\alpha 1}$ radiation from our rotating anode source and to analyse the x-rays scattered from the sample. With this configuration of the diffractometer the resolution in the scattering plane was typically 10^{-3} Å^{-1}. For the measurements of the critical x-ray scattering the germanium was replaced by pyrolytic graphite, giving a resolution of $\approx 10^{-2}$ Å^{-1}. The resolution perpendicular to the scattering plane in both configurations of the diffractometer was determined by slits to be $\approx 10^{-1}$ Å^{-1}.

The single crystal of $RbAlF_4$ used in our study was grown by the Bridgman technique. From a large boule a sample of approximately $(10 \times 10 \times 2)$ mm^3 was cleaved with the [001] direction normal to the largest face. (In what follows, unless otherwise stated, we shall index all planes and directions in the crystal with respect to phase I.) The very good quality of the cleaved face obviated the need to perform any special preparation of the surface.

The measurements were performed in reflection geometry, with the (010) plane in the scattering plane. For the measurements of the temperature dependences of the spontaneous strain and the super-lattice reflection intensity the crystal was mounted on the cold finger of a closed-cycle refrigerator. The temperature stability was monitored by a calibrated silicon diode and found to be better than 0.05 K. The critical scattering measurements were performed by placing the sample in a furnace with a stability as measured by a thermocouple of 0.1 K over the temperature range of 300 to 550 K. Great care was taken to ensure that the x-ray beam illuminated the same part of the crystal when it was transferred from the cryostat to the furnace, and to cross calibrate the silicon diode and the thermocouple.

3. Critical scattering theory

The x-ray scattering cross section for an x-ray wavevector transfer $\boldsymbol{Q}$ due to the X point soft mode, within the high-temperature, one-phonon approximation, is given by [14]

$$S(\boldsymbol{Q}) = k_B T \sum_{ij} \sum_{\boldsymbol{q}} F_i(\boldsymbol{Q}, \boldsymbol{q}) \chi_{ij}(\boldsymbol{q}) F_j(-\boldsymbol{Q}, -\boldsymbol{q}) \delta(\boldsymbol{Q} - \boldsymbol{G}_X - \boldsymbol{q}) . \qquad (1)$$

Formally, the sum ij is over all the normal modes of the lattice, but in the following we shall include only those two terms corresponding to rotations of the AlF_6^- octahedra around the [100] and [010] axes; the remaining modes are assumed to produce a wavevector independent background. In equation (1), $\chi_{ij}(\boldsymbol{q})$ is the static wavevector dependent susceptibility matrix, and has an anisotropy which directly reflects the anisotropy of the phonon dispersion surface at the X point. The one-phonon structure factor $F_i(\boldsymbol{Q},\boldsymbol{q})$ describes the coupling of the x-rays to the ith mode and can be written as

$$F_i(\boldsymbol{Q}, \boldsymbol{q}) = \sum_k f_k(\boldsymbol{Q}) \boldsymbol{Q} \cdot \boldsymbol{e}(\boldsymbol{k}, \boldsymbol{q}, \mathrm{i}) \exp\{\mathrm{i}[(\boldsymbol{Q} - \boldsymbol{q}) \cdot \boldsymbol{R}(k)]\} \qquad (2)$$

where the kth atom in the unit cell has a position vector $\boldsymbol{R}(k)$, a motion in the ith mode described by the eigenvector $\boldsymbol{e}(\boldsymbol{k}, \boldsymbol{q}, \mathrm{i})$, and a form factor $f_k(\boldsymbol{Q})$ which is defined so as to include the Debye–Waller factor. Although the soft mode at the X point is doubly degenerate, corresponding to rotations of the octahedra around either the [100]

or [010] axes, at a given X point only one of the two possible structure factors $F_x(\boldsymbol{Q},\boldsymbol{q})$ or $F_y(\boldsymbol{Q},\boldsymbol{q})$ is non-zero. For example, rotations of the AlF_6^- octahedra around [010] doubles the lattice parameter in the [1,0,0] direction, producing superlattice reflections at (0.5,0,0). Thus at this point we have $F_x(\boldsymbol{G}_X,0)=0$ and $F_y(\boldsymbol{G}_X,0)=F(\boldsymbol{G}_X)$.

The inverse of the static wavevector dependent susceptibility matrix $\chi_{ij}(\boldsymbol{q})$ is related to the frequency of the soft mode by

$$\chi_{ij}^{-1}(\boldsymbol{q})=\omega_{ij}^2(\boldsymbol{q}). \tag{3}$$

We can then expand the frequency as a Taylor series about $\boldsymbol{q}$=0, and use symmetry to reduce the number of coefficients. If we further assume that the coupling between rotations about [100] and [010] is negligible (that is we assume that the susceptibility matrix is diagonal) then for rotations about [010] we obtain to second order in $\boldsymbol{q}$

$$\omega_{yy}^2(\boldsymbol{q})=\omega_0^2(q=0,T)+\alpha_x q_x^2+\alpha_y q_y^2+\alpha_z q_z^2 \tag{4}$$

with a similar expression for rotations about [100]. The parameters α_x, α_y and α_z respectively characterize the phonon dispersion at the X point in the [100] (Γ–X line), [010] (X–M line) and [001] (X–R line) directions. The dispersion relations of the low-lying phonons in $RbAlF_4$ has been measured by Bulou *et al* [10] using neutron inelastic scattering. From their data we derive the values of the anisotropy parameters to be $\alpha_x=27.8(4.0)$, $\alpha_y=7.3(3.0)$ and $\alpha_z=38.9(9.0)$, all in units of THz^2 $Å^2$. The uncertainties on these parameters are large because the data of Bulou *et al* [10] are very sparse in the vicinity of the X point. In addition, their measurements were made at 400 °C, well above the temperature of our critical scattering measurements. However, as we shall show in the following section, our x-ray data indicate that the anisotropy of the phonon dispersion in $RbAlF_4$ is not strongly temperature dependent.

Combining the results given in equations (1) to (4), the x-ray scattering cross section at the X point in $RbAlF_4$ can be written as

$$S(\boldsymbol{Q})=k_B T|F(\boldsymbol{G}_X)|^2\sum_{\boldsymbol{q}}\frac{\chi(\boldsymbol{q}=0)\kappa^2}{(\kappa^2+q_x^2+a_1q_y^2+a_2q_z^2)}\delta(\boldsymbol{Q}-\boldsymbol{G}_X-\boldsymbol{q}). \tag{5}$$

Here $\chi(\boldsymbol{q}=0)$ is the static susceptibility, κ is the inverse correlation length of the soft-mode fluctuations, and $a_1=\alpha_y/\alpha_x$ with $a_2=\alpha_z/\alpha_x$.

The inverse correlation length is related to correlation length ξ by

$$\kappa=\frac{2\pi}{\xi}=\frac{\omega_0(q=0,T)}{\alpha_x^{1/2}}. \tag{6}$$

The temperature dependence of the inverse correlation length κ and the static $\chi(\boldsymbol{q}=0)$ susceptibility are expected to follow the conventional power laws

$$\kappa=\kappa_0[(T-T_{C2})/T_{C2}]^{\nu} \tag{7}$$

and

$$\chi(\boldsymbol{q}=0)=\chi_0[(T-T_{C2})/T_{C2}]^{-\gamma}. \tag{8}$$

It is also possible in an x-ray scattering experiment to measure the critical exponents β and $\tilde{\beta}$ characterizing respectively the temperature variation of the primary

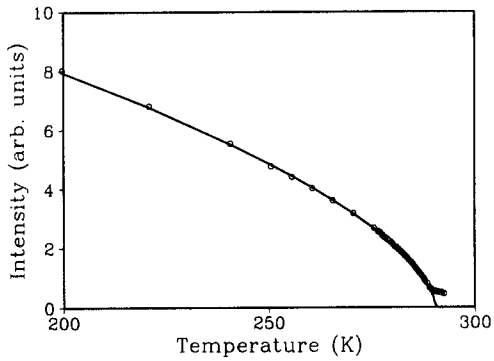

Figure 2. The temperature dependence of the integrated intensity (arbitrary units) of the superlattice reflection at (0.5,0,5). The full curve represents a least-squares fit to the power law $I = I_0[(T_{C2} - T)/T_{C2}]^{2\beta}$ with $T_{C2} = 290.5(5)$ K and $\beta = 0.305(20)$. The high-temperature tail above T_{C2} arises from critical diffuse scattering.

and secondary order parameters. For an improper ferroelastic transition, such as the tetragonal-to-orthorhombic transition in $RbAlF_4$, the intensity of the superlattice reflection, in this case at the X point, is directly proportional to the square of the primary order parameter. The secondary order parameter for such a transition is the spontaneous strain which develops below T_{C2}. In the limit of zero anisotropy, the critical exponents characterizing the transition at T_{C2} should be those of the $n = 2$, $d = 3$ XY model, as the soft mode is doubly degenerate.

From equation (5) it can be seen that the critical scattering is expected to be Lorentzian in reduced wavevector $\boldsymbol{q}$, with a width that depends on the direction of $\boldsymbol{q}$ with respect to the crystallographic axes. After convolving with the instrumental resolution function, the cross section given in equation (5) was used to fit our experimental results.

In deriving our expression for the x-ray scattering cross section, we have implicitly assumed that the atomic motions associated with the phase transition at T_{C1} have negligible effect on the critical scattering observed at the X point. This assumption greatly simplifies the expression for the cross section, and is justified by the fact that even at 293 K the M point superlattice reflections are very weak compared to those from phase I [9].

4. Experimental results and data analysis

4.1. Ordering curve

The first part of the experiment was devoted to the determination of the temperature dependence of the primary order parameter. This was performed by measuring the integrated intensity of the superlattice reflection at (0.5,0,5) (corresponding to the X point in the Brillouin zone of phase I) using the low-resolution, graphite configuration of the diffractometer as the sample was cooled below 300 K. As shown in figure 2, below approximately 290 K the intensity at this point increased smoothly with decreasing temperature, as expected for a second order transition. A fit of the intensity I to the conventional power law $I = I_0[(T_{C2} - T)/T_{C2}]^{2\beta}$, where β is the critical exponent of the primary order parameter, gave $T_{C2} = 290.5(5)$ K and $\beta = 0.305(20)$.

4.2. Spontaneous strain

The transition at T_{C2} is from the space group D_{4h}^5 to D_{2h}^{13} and can accordingly be classified as a ferroelastic transition. As a result a spontaneous strain characterizing the transformation from tetragonal to orthorhombic unit cells develops below T_{C2}. We define the strain S by

$$S = \frac{b_{III} - a_{III}}{b_{III} + a_{III}} \tag{9}$$

where the lattice parameters a_{III} and b_{III} refer to the orthorhombic unit cell (phase III), and a rotation of the AlF_6^- octahedra around the [010] axis was assumed so that $a_{III} \leq b_{III}$.

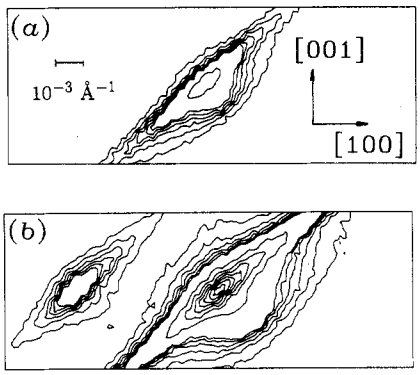

Figure 3. Intensity contour plots of the x-ray scattering measured in grid scans around the (305) reflection at (*a*) T_{C2} and (*b*) $(T_{C2} - 191)$ K.

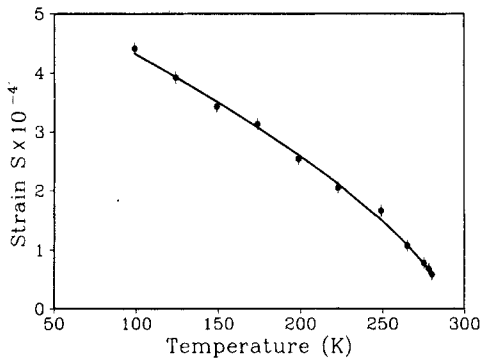

Figure 4. The temperature dependence of the spontaneous strain S determined by monitoring the domain splitting of the (305) Bragg peak. The full curve represents the result of a least-squares fit to the power law $S = S_0[(T_{C2} - T)/T_{C2}]^{2\tilde{\beta}}$; with T_{C2} held fixed at 290.5 K we obtained $\tilde{\beta} = 0.343(10)$.

In $RbAlF_4$ the spontaneous strain can be deduced from the splitting below T_{C2} of the tetragonal Bragg reflections along [100]. As this splitting is expected to be very

small [10], our measurements were performed using the high-resolution, germanium configuration of the diffractometer. In figure 3 we show intensity contour plots of the scattering measured in grid scans around the (305) reflection at T_{C2} and at (T_{C2} − 191) K (a high-h Miller index reflection was chosen for study as the observed splitting is directly proportional to h). The thermal evolution of the spontaneous strain is shown in figure 4. Unfortunately, even with the high-resolution configuration, the peak splitting of the (305) for temperatures within 10 K of T_{C2} were too small to be resolved. The full curve in figure 4 represents the result of a least-squares fit to the power law $S = S_0[(T_{C2} - T)/T_{C2}]^{2\tilde{\beta}}$ where the $\tilde{\beta}$ is the critical exponent describing the secondary order parameter. The best fit to the data gave $T_{C2} = 292(4)$ K and $\tilde{\beta} = 0.351(20)$, whereas with the value of T_{C2} held fixed at 290.5 K, we obtained $\tilde{\beta} = 0.343(10)$.

4.3. Critical scattering

The wavevector dependence of the critical scattering was determined above T_{C2} around the point (0.5,0,5) using the low-resolution, graphite mode of the instrument. A typical pair of scans along [100] and [001] through the point (0.5, 0, 5) at 301.5 K is shown in figure 5. The general trend in the scattering at the X point was for its width to decrease and its intensity to increase as the temperature was lowered towards T_{C2}, as expected for a second-order phase transition.

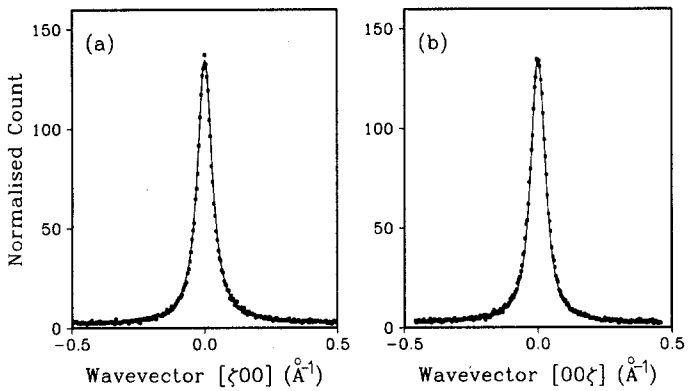

Figure 5. The x-ray critical scattering observed around (0.5, 0, 5) for scans along (*a*) the [100] and (*b*) the [001] directions of phase I at 301.6 K. The full curves are the results of least-squares fits (goodness of fit per degree of freedom, $\chi^2 = 1.9$) to an anisotropic Lorentzian scattering model, convolved with the instrumental resolution function. The parameters varied in the fit were the static susceptibility $\chi(q = 0)$, inverse correlation length κ, a flat background and two parameters which allowed for any small offsets in the centres of the scans.

The full curves in figure 5 represent the result of a least-squares fit of our anisotropic Lorentzian scattering model, convolved with the instrumental resolution, to the data. Pairs of scans along the [100] and [001] directions were fitted simultaneously. The only parameters allowed to vary in the fit were the static susceptibility $\chi(q = 0)$, inverse correlation length κ of the soft-mode fluctuations, two parameters allowing for any small offsets in the centre of the scans and a flat background; the

anisotropy parameters were held fixed at the values $a_1 = 0.26$ and $a_2 = 1.40$ (see section 3). The background was also held fixed in final fits to the data. In fitting the data we assumed that the out-of-plane resolution function was triangular, thus enabling the convolution integral over the out-of-plane component of $\boldsymbol{q}$ to be performed analytically. This considerably speeded up the computations. For the data taken at 301.5 K, a comparison of the parameters obtained using this method with those deduced from a full three dimensional convolution of the resolution function showed no significant discrepancies. The instrumental resolution function was estimated from the widths of the Bragg peak at $(0.5, 0, 5)$ below T_{C2}.

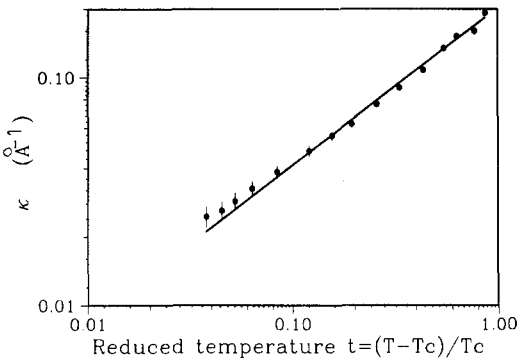

Figure 6. The temperature dependence of the inverse correlation length κ deduced from anisotropic Lorentzian fits to the data. The full line is the result of a fit to the power law given in equation (7); with T_{C2} held fixed at 290.5 K, $\nu = 0.64(2)$.

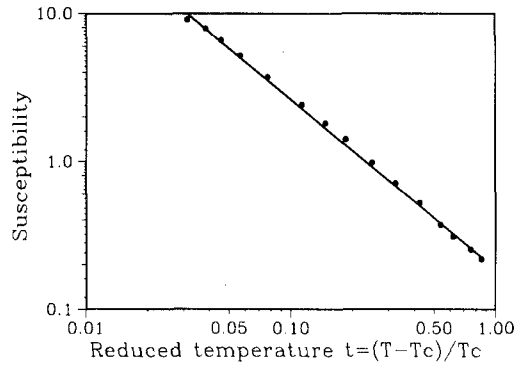

Figure 7. The temperature dependence of the static susceptibility $\chi(\boldsymbol{q} = 0)$ deduced from anisotropic Lorentzian fits to the data . The full line is the result of a fit to the power law given in equation (8); with T_{C2} held fixed at 290.5 K, $\gamma = 1.15(6)$.

The temperature dependences of the inverse correlation length κ and the static susceptibility $\chi(\boldsymbol{q} = 0)$ obtained from fits to our scattering model are shown respectively in figures 6 and 7. The full lines in these figures represent the results of least-square fits to the power laws given in equations (7) and (8), and with T_{C2} held fixed at 290.5 K, they have critical exponents $\nu = 0.64(2)$ and $\gamma = 1.15(6)$.

5. Discussion and conclusions

5.1. Order parameter

The order parameter of the tetragonal-to-orthorhombic phase transition in $RbAlF_4$ has been determined in two ways. Firstly, the temperature dependence of the primary order parameter was obtained by monitoring the integrated intensity of the superlattice reflection at (0.5,0,5), and is described by a power law with critical exponent $\beta = 0.305(20)$ and $T_{C2} = 290.5(5)$ K. Secondly, the secondary order parameter was deduced from the domain splitting of the (305) Bragg peak, and has a temperature dependence described by the critical exponent $\tilde{\beta} = 0.351(20)$ with $T_{C2} = 292(4)$ K. Both methods used to obtain the order parameter have, however, their own limitations. In the first case, the inferred value of β is affected not only by extinction but also by any variation in the relative populations of the two domain types with temperature. Additionally, the apparent transition temperature is affected by the presence of the diffuse scattering tail above T_{C2}. In the second case, even using high resolution we were only able to measure the splitting below $\approx (T_{C2} - 10)$ K, thus preventing us from accurately determining the transition temperature.

In view of these shortcomings, our values for β and $\tilde{\beta}$ can be considered to be in reasonable agreement with the theoretical value for the isotropic $n = 2$, $d = 3$ model of $\beta = 0.345(2)$ [15]. Moreover, it is interesting to note that our values for the primary and secondary order parameters obey the expected inequality $\tilde{\beta} \geq \beta$ [14]. The transition temperatures determined from the two techniques are consistent with each other and with the value $T_{C2} = 292$ K obtained from powder diffraction [9], but are significantly greater than that deduced from linear birefringence measurements of $T_{C2} = 282$ K [16]. We do not know the reason for this discrepancy.

5.2. Critical scattering

We see from figure 5 that the measured wavevector dependence of the critical scattering is well described by the anisotropic Lorentzian cross section developed in section 3. Thus, our assumption that the transition at T_{C1} can effectively be ignored in deriving the cross section at the X point appears to be valid. The observed anisotropy of the scattering in the diffraction plane is in good agreement with the value we deduced for a_2 from the phonon dispersion curves measured by Bulou *et al* [10]; the poor instrumental perpendicular to the scattering plane means that our fits are not very sensitive to the parameter a_1. We can therefore conclude that, at least between 400 °C and room temperature, the anisotropy in the phonon dispersion at the X point in $RbAlF_4$ is not very temperature dependent.

The temperature dependence of the inverse correlation length κ and static susceptibility $\chi(q = 0)$ of the soft-mode fluctuations fit reasonably well to the expected power laws, with respective critical exponent ν=0.64(2) and γ=1.15(6). These values are consistent with field theory calculations for the $n = 2$, $d = 3$ model which give ν=0.669(3) and γ=1.316(3) [15]. However, a generally accepted working rule of thumb in the study of critical phenomena is that in order to obtain accurate critical exponents it is necessary perform measurements over at least two orders of magnitude in reduced temperature t, and preferably three. The temperature stability of our furnace was very poor below $\approx$ 300 K with an equilibration times in excess of 12 h, and we were unable to obtain reliable data below this temperature, thus failing to satisfy the above criterion. Our measurements cannot therefore be considered as an accurate

determination of the critical exponents as such, but they are clearly in agreement with the expected theoretical behaviour.

Finally, we consider briefly our failure to find any evidence for an anomalous second component in the length scales of the critical fluctuations in $RbAlF_4$. At present it is thought that the second length scale in the perovskites arises from the effect of random fields, generated by defects (of an unspecified type), on a weakly first-order transition, as originally considered by Imry and Wortis [17]. In this model, the defects stabilize clusters of the low-temperature phase in the high-temperature, cubic phase, and it is the fluctuations in the size of these clusters which gives rise to the observed second length scale. Thus, we can plausibly interpret our failure to observe a second length scale in $RbAlF_4$ as being due either to the fact that the transition is truly continuous, in which case it would not be possible for clusters of the low-temperature phase to develop above T_{C2}, or that the defect concentration in our sample was too low to produce a measurable density of clusters. (As far as the latter is concerned, we note that the mosaic spread of our sample was 0.009°. This value is intermediate between the mosaic spread of the $RbCaF_3$ crystal II (0.012°), which displayed the second length scale, and crystal I (0.005°) which did not [3–5].) Clearly, further studies on crystals of $RbAlF_4$ of varying perfection, or with controlled quantities of substitutional impurities, would be useful to help shed some light on this intriguing problem.

Acknowledgments

We gratefully acknowledge the unflagging technical support provided by Hugh Vass and Deborah Hardy. We have also benefited greatly from discussions with Professor R A Cowley, Dr A D Bruce and Dr A Bulou. The excellent single crystal used in this study was grown by Dr J Nouet with the technical assistance of G Miesseron, to both of whom we would like to extend our thanks. Our work was supported by a research grant from the Science and Engineering Research Council, the British Council and NATO (grant No 0477187).

References

[1] Andrews S R 1986 *J. Phys. C: Solid State Phys.* **19** 3721
[2] Nelmes R J, Hatton P D and Vass H 1988 *Phys. Rev. Lett.* **60** 2172
[3] Ryan T W, Nelmes R J, Cowley R A and Gibaud A 1986 *Phys. Rev. Lett.* **56** 2704
[4] Gibaud A, Ryan T W and Nelmes R J 1987 *J. Phys. C: Solid State Phys.* **20** 3833
[5] Gibaud A, Cowley R A and Mitchell P W 1987 *J. Phys. C: Solid State Phys.* **20** 3849
[6] Nicholls U J and Cowley R A 1987 *J. Phys. C: Solid State Phys.* **20** 3417
[7] Cochran W 1960 *Adv. Phys.* **9** 387
[8] Bulou A 1985 *PhD Thesis* University of Le Mans
[9] Bulou A and Nouet J 1982 *J. Phys. C: Solid State Phys.* **15** 183
[10] Bulou A, Rousseau M, Nouet J and Hennion B 1989 *J. Phys.: Condens. Matter* **1** 4553
[11] Launay J M, Bulou A, Hewat A W, Gibaud A, Laval J Y and Nouet J 1985 *J. Physique* **46** 771
[12] Gibaud A, Bulou A, Le Bail A, Nouet J and Zeyen C M E 1987 *J. Physique* **48** 1521
[13] Bulou A, Leble A, Hewat A and Fourquet J L 1982 *Mater. Res. Bull.* **17** 391
[14] Bruce A D and Cowley R A 1981 *Structural Phase Transitions* (London: Taylor and Francis)
[15] Le Guillou J C and Zinn-Justin J 1981 *Phys. Rev.* B **21** 3976
[16] Kleemann W, Schafer F J and Nouet J 1982 *J. Phys. C: Solid State Phys.* **15** 197
[17] Imry Y and Wortis M 1979 *Phys. Rev.* B **19** 3580